Reliability Assessment of Internal Stability Limit States for Two As-Built Geosynthetic MSE Walls

Richard J. Bathurst, *Ph.D., P.Eng, Professor, Department of Civil Engineering, GeoEngineering Center at Queen's-RMC, Royal Military College of Canada, Kingston, ON, Canada; email: bathurst-r@rmc.ca*
Tony M. Allen, *M.Sc., P.E, State Geotechnical Engineer, Washington State Department of Transportation, Olympia, WA, U.S.A.; email: allent@wsdot.wa.gov*

ABSTRACT: *This paper reports the results of calculations for the margins of safety for internal stability limit states for two as-built geosynthetic MSE walls constructed in 2006 in Washington State, U.S.A. The walls are unique because a) the internal stability design for the reinforcement was based on a working stress design method which includes the stiffness of the reinforcement as a key parameter, and b) the walls were instrumented and monitored during and after construction. Margins of safety are quantified deterministically using factors of safety, and probabilistically using reliability indices. The calculations are performed using the properties of the as-built materials as opposed to the properties assumed at the time of original design. The results show that the margins of safety for tensile and pullout strength are huge and thus these limit states are not of practical concern for these structures. The critical limit state is the soil failure limit state. Margins of safety for this limit state are shown to be closer to recommended minimums but nevertheless adequate for all reinforcement layers in both walls.*

KEYWORDS: Geosynthetic reinforcement, MSE walls, SR-18 walls, internal limit states, reliability, factor of safety, tensile strength, pullout strength, soil failure

SITE LOCATION: Geo-Database

INTRODUCTION

Two modular block geosynthetic mechanically stabilized earth (MSE) walls were constructed in 2006 to support the approach embankment for a pair of highway bridges crossing the Cedar River near Maple Valley in Washington State, U.S.A. (Allen and Bathurst 2014a,b). The project was unique because a) the internal stability design for the reinforcement was based on a new working stress design method called the K-stiffness Method (Allen et al. 2003; Bathurst et al. 2005), and b) the walls were instrumented and monitored during and after construction. A key feature of the design method is the use of the reinforcement stiffness to estimate tensile loads in the reinforcement layers under operational conditions. Prior to this method, the magnitudes of reinforcement load in U.S. practice were computed using the AASHTO Simplified Method (e.g., AASHTO 2017) which is a conventional tie-back wedge method in which active earth pressures are distributed to the reinforcement layers according to the reinforcement spacing and depth regardless of the reinforcement strength or stiffness properties. The original K-stiffness Method has undergone minor refinements and is now known as the Simplified Stiffness Method (Allen and Bathurst 2015), or the Stiffness Method in current AASHTO (2020) specifications.

The Stiffness Method and its antecedents have been proven to give more accurate estimates of reinforcement loads in MSE walls under operational conditions compared to typically larger (more conservative) estimates using the Simplified Method. A practical benefit of the (Simplified) Stiffness Method over the Simplified Method for design is that the amount of reinforcement required for internal stability limit states design of geosynthetic MSE walls is less and the reinforcement layers are located more efficiently (e.g., Allen et al. 2015, 2019). In addition, the method is seamless across relatively extensible geosynthetic reinforcement materials (i.e., geotextiles, geogrids, and polyester straps) and relatively inextensible steel reinforcement materials (e.g., steel strips and grids). The reinforcement loads recorded for the two SR-18 walls in this study

Submitted: 18 November 2020; Published: 25 October 2021
Reference: Bathurst R. J., and Allen T. M. (2021). Reliability Assessment of Internal Stability Limit States for Two As-Built Geosynthetic MSE Walls. International Journal of Geoengineering Case Histories, Volume 6, Issue 4, pp. 67-84, doi: 10.4417/IJGCH-06-04-05

have been collected along with measurements from many other walls to assess the accuracy of the Simplified and Stiffness Methods, and to judge the veracity of numerical model predictions of the performance of these two structures (Yu et al. 2016).

The objective of this paper is to estimate the design margins of safety for three internal stability limit states for the two as-built SR-18 walls based on deterministic (factor of safety) and probabilistic (reliability) approaches. The three limit states addressed are tensile strength (rupture), pullout strength, and soil failure. The paper demonstrates that the soil failure limit state is the most critical limit state. Analyses are repeated using a hypothetical lower strength and stiffness geogrid for one of the walls to investigate the possibility of reducing the excessive margins of safety for the tensile strength and pullout limit states for the original wall, while keeping all other properties and geometry the same as the original structure.

SR-18 WALLS

A cross section view of the two walls is shown in Figure 1. Wall D was 10.7 m high and Wall C was 6.3 m high. A photograph of the taller Wall C is depicted in Figure 2. The internal reinforcement arrangement and type are shown in Figure 3. Three different integral punched and drawn high density polyethylene (HDPE) geogrids were used in the design of Wall C. The strength and stiffness of these three materials increased in the order of HDPE-1, HDPE-2 and HDPE-3. Geogrid HDPE-1 was used for Wall D but was found to have a slightly different stiffness when tested as compared to the material with the same product designation for Wall C. The details of the project construction and design have been reported by Allen and Bathurst (2014a,b). The properties of the as-built geogrid products differed from the original design and there were differences between the soil properties assumed at time of the original design and construction. The authors compared predicted loads using the K-stiffness Method for the original design and for the as-built walls in the earlier related papers (Allen and Bathurst 2014a,b). In the current study, the as-built properties of the reinforcement and soil backfill are used and these properties are summarized in Table 1.

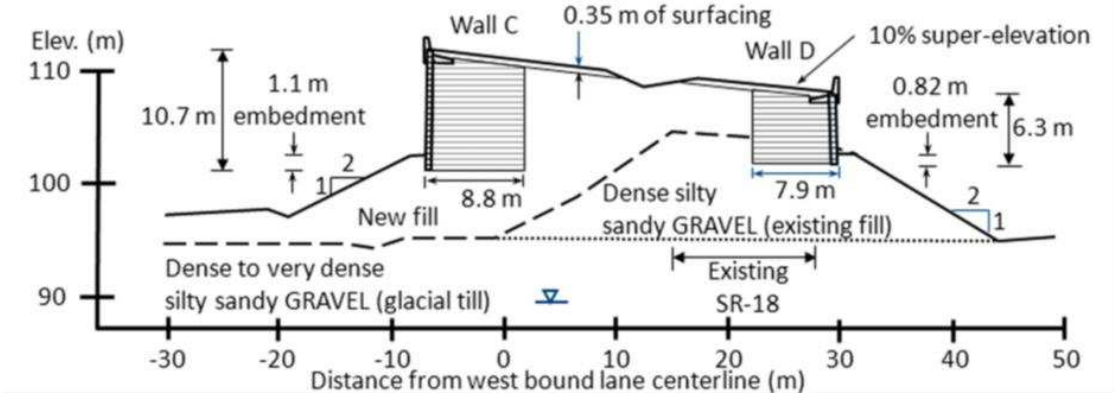
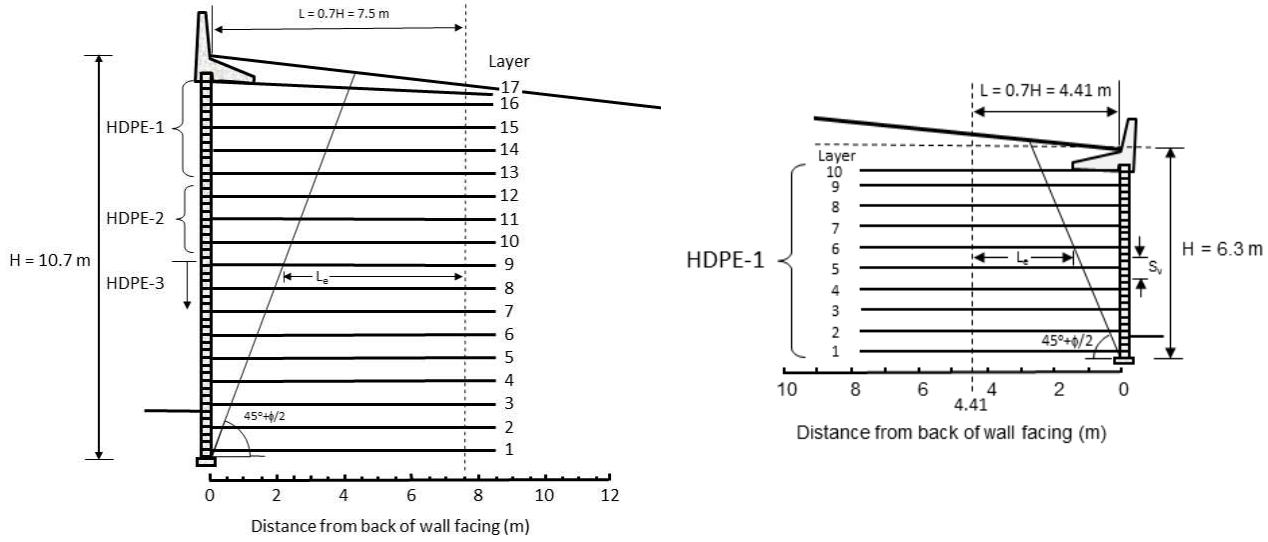


Figure 1. Cross-section view of back-to-back geogrid reinforced MSE walls (Allen and Bathurst 2014b).



Figure 2. Photograph of 10.7 m-high MSE wall (Wall C) (Allen and Bathurst 2014a).



a) Wall C *b) Wall D*

Figure 3. Cross-section views of SR-18 walls.

Table 1. As-built geometry and material properties for Walls C and D (Allen and Bathurst 2014a,b).

Parameter	Wall D	Wall C
Height, H (m)	6.3 (6.1) *	10.7 (10.5) **
Soil friction angle, ϕ (°)	47	47
Bulk soil unit weight, γ (kN/m^3)	22.0	22.0
Soil cohesion (kPa)	0	0
Equivalent uniform surcharge height, S (m)	0.23	0
Thickness of the facing column (m)	0.305	0.305
Facing block unit weight (kN/m^3)	18.85	18.85
Facing stiffness factor Φ_{fs} ***	0.75	1.0
Tributary vertical spacing of reinforcement layers, S_v (m)	0.5 for the top layer; 0.6 for other layers	0.7 for the top layer; 0.6 for other layers
Reduction factor, RF	3.6	3.6
Reinforcement designation	HDPE-1	HDPE-1, HDPE-2, HDPE-3
Ultimate tensile strength, T_{ult} (kN/m)	62.5	62.5, 71.2, 117
Tensile strength at end of design life, T_{al} (kN/m)	17.4	17.4, 19.8, 32.5
Reinforcement stiffness, $J_{2\%}$ (kN/m) ****	232	246, 393, 598

* Analyses carried out for lower wall height before final paving was completed one year later.
** Value in parentheses is corrected value used in calculations to account for negative slope at backfill surface.
*** Wall D is shorter than Wall C and thus the facing column is less flexible. This leads to a lower facing stiffness factor which in turn leads to lower reinforcement loads when all other factors are the same (see Allen and Bathurst 2015).
**** At end of construction.

COMPARISON OF PREDICTED AND MEASURED LOADS

The SR-18 project allowed the predicted maximum tensile loads in the reinforcement to be compared to measured maximum loads recorded at instrumented layers. These comparisons are shown in Figure 4. The measured values are at locations in the backfill away from the connections and at monitoring points close to the connections. The measured values in the backfill are judged to be in good agreement with predicted values using the Simplified Stiffness Method where these comparisons can be made. There are greater differences at the connections. Nevertheless, predicted values using the Stiffness Method are much closer to all measured values than those using the AASHTO (2017, 2020) Simplified Method; the latter are conservative

in all cases and often by large amounts. The excessive conservativeness in predicted maximum tensile load has been noted in prior related work by the authors based on analyses of 85 full-scale instrumented field structures with 449 load measurements (e.g., Allen and Bathurst 2015; Miyata et al. 2018) and 665 reinforcement load measurements from 16 full-scale instrumented laboratory models constructed at the Royal Military College of Canada (e.g., Bathurst et al. 2000). Bathurst et al. (2019a) reported that for vertical or near-vertical geosynthetic MSE walls, measured T_{max} values were *on average* 25% of the values predicted using the Simplified Method, and the spread in the ratio of measured to predicted values (i.e., bias) was 66%. By comparison, the Stiffness Method slightly overestimates the measured (observed) maximum tensile loads (on average), and the spread in values (coefficient of variation) is only 36% as shown in Table 2.

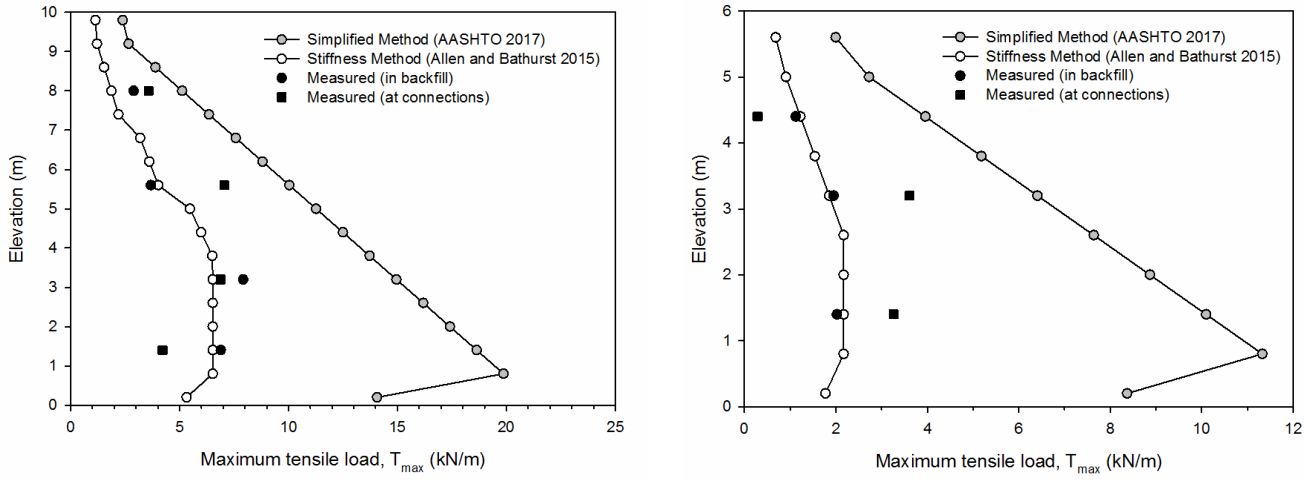


Figure 4. Predicted and measured maximum tensile loads at end of construction.

Table 2. Summary of bias statistics and bias dependency values for load and resistance models for geogrid reinforced soil walls constructed with granular soil.

Model (AASHTO 2020)	Model equation	Number of data points	Mean of bias	COV of bias	Bias dependency	Data source
Load model	Equation 1a and 1b	96	$\mu_{\lambda Q} = 0.96$	$COV_{\lambda Q} = 0.36$	$\rho_Q = 0.09$ *	Allen and Bathurst (2015)
Tensile rupture	Equation 2	N/A	$\mu_{\lambda R} = 1.10$	$COV_{\lambda R} = 0.10$	$\rho_R = 0$	Bathurst et al. (2011, 2019)
Pullout model	Equation 3	318	$\mu_{\lambda R} = 2.23$	$COV_{\lambda R} = 0.55$	$\rho_R = -0.46$	Huang and Bathurst (2009)
Soil failure	Equation 4	8	$\mu_{\lambda R} = 1.01$	$COV_{\lambda R} = 0.14$	$\rho_R = 0$	Allen and Bathurst (2019)

* $\rho = 0$ at level of significance of 5%, and this value is used in numerical calculations. N/A = not available.

INTERNAL LIMIT STATES

In this paper, internal stability limit states for tensile strength (rupture), pullout strength, and soil failure are investigated. The geometry and parameters that correspond to these limit states are found in Figure 5. An assessment of the connection strength limit state is not attempted (i.e., the connection between the reinforcement and the wall facing) because connection capacity bias values are not available at the time of the current study.

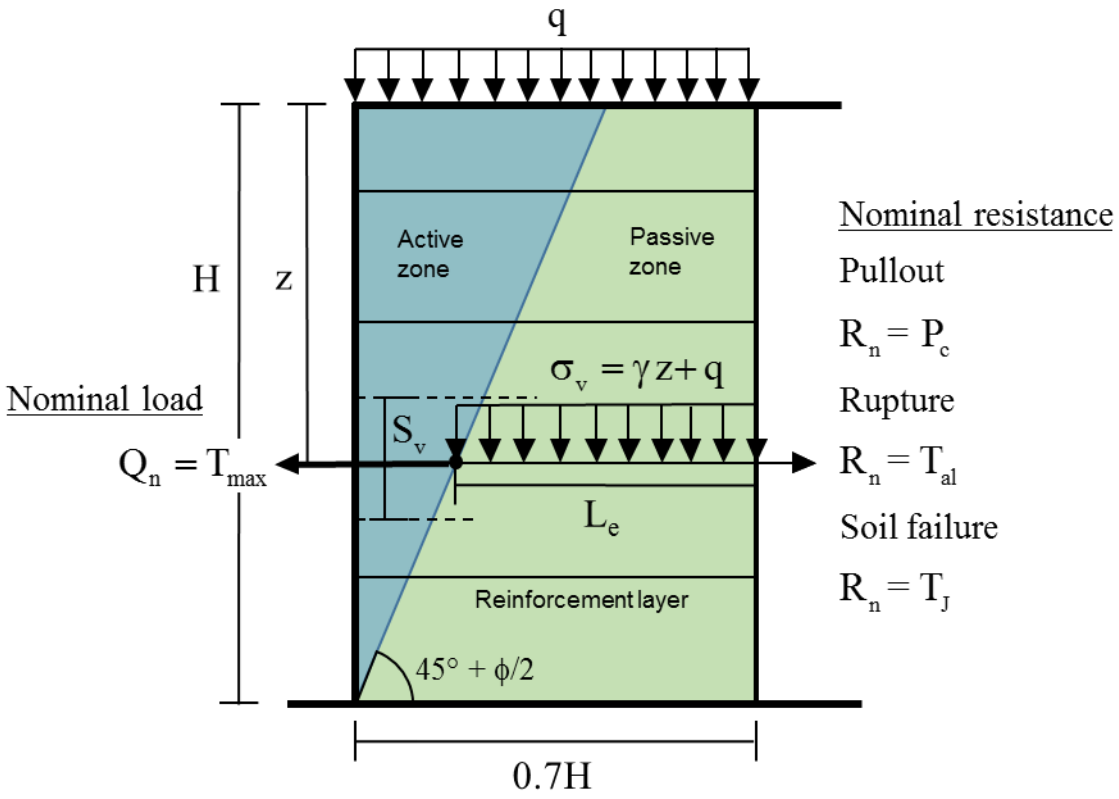


Figure 5. Internal stability limit states.

Tensile Load

The calculation of nominal load (T_{max}) for a reinforcement layer is based on the (Simplified) Stiffness Method (Allen and Bathurst 2015, 2018) which has been adopted in the AASHTO (2020) LRFD specifications in the U.S.A. The equation for T_{max} found in the cited references is a function of the input parameters shown below:

$$T_{max} = f(H, \omega, \Phi_{fs}, S_v, z, \varphi, c, \sigma_V, J) \tag{1a}$$

Here, T_{max} is the maximum tensile load in a reinforcement layer under operational conditions and is expressed in units of force per unit running length of wall face (e.g., kN/m). Other terms are H = height of wall, ω = facing batter from vertical, Φ_{fs} = facing stiffness factor, S_v = tributary area of each reinforcement layer, z = depth of layer below crest of the wall, ϕ = peak friction angle of the soil, c = soil cohesion, σ_v = vertical stress due to soil self-weight (γ) plus any uniformly distributed surface surcharge q (i.e., $\sigma_v = \gamma z + q$), and J = secant tensile stiffness value at 2% strain and 1000 h for geotextiles and geogrids (Allen and Bathurst 2015) and 1% strain and 1000 h for polyester straps (Miyata et al. 2018). The actual expression for T_{max} in the references cited includes non-dimensional factors which are collections of the parameters shown above, hence:

$$T_{max} = \frac{1}{2} K (H + S) \gamma S_v D_{tmax} \Phi_g \Phi_{local} \Phi_{fs} \Phi_{fb} \Phi_c \tag{1b}$$

where, K = index lateral earth pressure coefficient for the reinforced soil and is set equal to $K_a = (1-\sin\phi)/(1+\sin\phi)$, S = equivalent surcharge height using the reinforced soil unit weight = q/γ, D_{tmax} = distribution factor to estimate T_{max} for each layer as a function of layer depth and the maximum reinforcement load in the wall from all layers, Φ_g = global reinforcement stiffness factor, Φ_{local} = local reinforcement stiffness factor, Φ_{fb} = facing batter factor, Φ_{fs} = facing stiffness factor (as before), Φ_c = soil cohesion factor, and all other parameters have been defined above. For the two walls that are the subject of this paper, c = ω = 0 in Equation 1a which results in $\Phi_{fb} = \Phi_c = 1$ in Equation 1b.

Tensile Strength

The ultimate tensile strength (rupture) capacity of the reinforcement is taken as the long-term strength (T_{al}) and is computed as (AASHTO 2020):

$$T_{al} = \frac{T_{ult}}{RF} = \frac{T_{ult}}{RF_{ID} \times RF_{CR} \times RF_D} \quad (2)$$

The numerator is a reference laboratory ultimate tensile strength (T_{ult}) that is reduced by factors that account for loss of strength over the design life of the reinforcement due to installation damage (RF_{ID}), creep (RF_{CR}), and degradation (durability) mechanisms (RF_D). Parameter RF is the combined reduction factor.

Pullout Strength

The ultimate pullout capacity (P_c) in this paper is computed using the current AASHTO (2020) model expressed as:

$$P_c = 2F^* \alpha L_e \sigma_v R_c \leq T_{ult} \quad (3)$$

Here, F* = coefficient of interaction (dimensionless) = (2/3) tanϕ, α = 0.8, L_e = anchorage length within the passive zone (Figure 5), and R_c = reinforcement coverage ratio which is $R_c \leq 1$. The maximum value of pullout strength is capped at the ultimate tensile strength of the reinforcement. This limit can be observed in the laboratory when pullout box tests are carried out with large vertical confining pressures and the reinforcement ruptures at the external loading clamp located in air beyond the pullout box (Huang and Bathurst 2009).

Soil Failure Limit State

A unique feature of the Stiffness Method is the soil failure limit state, which is a calculation check to ensure that the soil in the reinforced zone remains at working stress conditions. The Stiffness Method is used to compute reinforcement loads under wall operational conditions consistent with notions of working stress as opposed to limit equilibrium conditions when the soil is at incipient failure. If an extensible (geosynthetic) reinforcement layer is allowed to strain excessively, then the soil will fail. This is called a "failure" limit state because it is consistent with the soil failing in shear (i.e., the shear strength of the soil is exceeded but the strength of the reinforcement is not), but in application it is a serviceability limit state (AASHTO 2020). If this serviceability limit state is not satisfied, then slumping and cracking of the backfill soil, facing outward movements, and continuing reinforcement creep may occur and thus compromise the performance of the wall under operational conditions, but the wall does not collapse.

The examination of the large number of instrumented and monitored full-scale walls collected by the writers during the development of the Stiffness Method showed that for geosynthetic walls constructed with granular fills, soil failure was minimized by keeping geosynthetic strains to less than ε_{max} = 2.5% to 3% and the average strain in all layers to less than 2% for walls constructed with a hard facing (Allen and Bathurst 2002, 2013, 2018). In the current AASHTO (2020) specifications, the maximum strain is limited to 2% for stiff-faced walls to be conservative. The maximum tensile load to satisfy the soil failure limit state is computed as:

$$T_J = J_{2\%} \times \varepsilon_{max} \quad (4)$$

where $J_{2\%}$ is the isochronous secant tensile stiffness corresponding to 2% strain and 1000 h. Details of the method to determine this stiffness value and the choice of the 2% strain value and 1000 h can be found in the paper by Allen and Bathurst (2019). It should be noted that this limit state only applies to the Stiffness Method because this criterion is linked to reinforcement stiffness. Reinforcement stiffness and strain level are not considered explicitly in the calculation of T_{max} for geosynthetic MSE walls using the Simplified Method (AASHTO 2017; CSA 2019) and variants that are based on conventional notions of active earth theory.

METHODOLOGY FOR RELIABILITY ANALYSES

The limit state functions in this investigation are expressed as:

$$g = \frac{\lambda_R R_n}{\lambda_Q Q_n} - 1 \tag{5}$$

Here R_n and Q_n are nominal resistance and load terms, and λ_R and λ_Q are the corresponding bias values. Bias is the ratio of measured (observed) value to predicted value. Nominal and bias values are treated as random values. The probability that a limit state is not satisfied (i.e., $P_f = P(g < 0)$) can be computed using Monte Carlo simulation. Alternatively, the margin of safety in probabilistic terms can be expressed by reliability index β. The link to probability of failure is $P_f = 1 - \Phi(\beta)$, where $\Phi(\beta)$ is the standard normal cumulative distribution function (NORMSDIST(β) in Excel). Fortunately, there is a closed-form solution for reliability index (β) that can be used to estimate the margin of safety in probabilistic terms for the case of simple linear limit state functions with a single load term (Q_n) and all bias and nominal values are lognormal distributed (the typical case); specifically (Bathurst and Javankhoshdel 2017):

$$\beta = \frac{ln\left[\left(\frac{\mu_{\lambda R}\mu_{Rn}}{\mu_{\lambda Q}\mu_{Qn}}\right)\sqrt{\frac{(1+COV_{Qn}^2)(1+COV_{\lambda Q}^2)}{(1+COV_{Rn}^2)(1+COV_{\lambda R}^2)}}\right]}{\sqrt{ln\left[\frac{(1+COV_{Qn}^2)(1+COV_{\lambda Q}^2)(1+COV_{Rn}^2)(1+COV_{\lambda R}^2)(1+\rho_R COV_{Rn} COV_{\lambda R})^2(1+\rho_Q COV_{Qn} COV_{\lambda Q})^2}{(1+\rho_n COV_{Rn} COV_{Qn})^2}\right]}} \tag{6}$$

This equation follows from basic probability theory. All assumptions and full details of its derivation can be found in the appendix to the paper by Bathurst and Javankhoshdel (2017). Parameters μ_{Rn}, μ_{Qn}, $\mu_{\lambda R}$, and $\mu_{\lambda Q}$ are mean values of nominal resistance and load values (R_n and Q_n), and resistance and load bias values (λ_R and λ_Q), respectively. Their corresponding coefficients of variation (COV) are denoted as COV_{Rn}, COV_{Qn}, $COV_{\lambda R}$, and $COV_{\lambda Q}$. The nominal resistance value (R_n) and nominal load value (Q_n) used at time of design in the limit state design equations are equivalent to μ_{Rn} and μ_{Qn} in the above equation. Lognormal distributions for load and resistance bias values for the internal limit states of MSE walls constructed with extensible (geosynthetics) and inextensible (steel) reinforcement materials have been demonstrated to satisfactorily approximate, at least visually, cumulative distribution function (CDF) plots for these data over the range of bias values that influence probabilistic calculation outcomes (e.g., Bathurst et al. 2019a,b, 2020a; Bozorgzadeh et al. 2020).

The COV values for nominal load and resistance values (Q_n and R_n) capture the total uncertainty in the magnitude of nominal values used at time of design from all sources. For example, there is always some uncertainty in the value of friction angle and unit weight that appear in the load and pullout equations introduced earlier. The assumption that distributions for nominal load and resistance values are lognormal distributed is expected because when the distributions for soil unit weight and friction angle (which are best described by lognormal distributions to avoid negative values during MC sampling) are included in stochastic estimates of the nominal values using these equations, the nominal values will also be lognormal distributed.

However, the sources of uncertainty can extend to the applicability of the load and resistance models to project-specific conditions. In Canadian load and resistance factor design (LRFD) foundation practice, the concept of "level of understanding" has been adopted (CSA 2019). The magnitude of resistance factor used in a limit state design equation in the Canadian LRFD code increases as the level of understanding moves from low to high. The level of understanding grows with increasing amount and quality of project materials data as well as with the greater experience of the designer with the candidate MSE wall technology, and alternatively decreases with increasing complexity of the project and so on. The three levels of understanding that appear in the Canadian code are used to reward design engineers (and their clients) with more cost-effective design solutions as more effort is expended to increase project level of understanding. Stated alternatively, this scheme encourages engineers to collect more site information and to carry out more material property testing.

In order to quantify level of understanding in reliability-based analysis and design, Bathurst et al. (2017) mapped COV of nominal values of 0.1, 0.2, and 0.3 to high, typical, and low levels of understanding, respectively. The choice of level of understanding for a project is subjective and based on judgment and experience. Hence, the choice of COV = 0.1, 0.2, or 0.3 is subjective. However, this range of COV values has been identified as typical for geotechnical foundation design by Becker

(1996). Recall also that the reinforced soil and the reinforcing elements are engineered materials, which reduces uncertainty in the estimate of nominal load and resistance values at time of design compared to foundation structures constructed on or in natural soil deposits (e.g., see Phoon and Tang 2019). Bathurst et al. (2017) provide an example template for the pullout limit state to assist the designer to select an appropriate project-specific "level of understanding."

The exception to COV of nominal values of 0.1, 0.2, and 0.3 that are used in the calculations that appear later in the paper is the tensile rupture limit state. For this limit state, $COV_{Rn} = 0$ because the nominal long-term tensile strength of the reinforcement (T_{al}) used at time of design is prescribed based on project conditions and reinforcement type. The uncertainty (or variability) in long-term tensile capacity of the reinforcement is captured entirely by the spread in bias values (i.e., $COV_{\lambda R}$) that is computed from variability in tensile strength at end of design life.

The first item in the numerator of Equation 6 is called the operational factor of safety:

$$OFS = \frac{\mu_{\lambda R}\mu_{Rn}}{\mu_{\lambda Q}\mu_{Qn}} = \frac{\mu_{\lambda R}}{\mu_{\lambda Q}} \times F_n \tag{7}$$

Inspection of this equation shows that the average operational factor of safety is different from the nominal factor of safety, F_n. Typically, OFS > F_n because resistance models often underestimate resistance capacity and/or load models tend to overestimate actual loads.

Parameters ρ_R and ρ_Q in Equation 6 are Pearson's correlation coefficients between variables R_n and λ_R, and between Q_n and λ_Q, respectively, and represent bias dependencies with nominal values. Stated alternatively, these correlations capture the case where model accuracy (i.e., bias) varies with the magnitude of the computed nominal value. Parameter ρ_n is the correlation coefficient between R_n and Q_n and is called nominal correlation following the terminology introduced by Lin and Bathurst (2018).

Equation 6 can be written as:

$$\beta = A \times ln(F_n) + B \tag{8}$$

where A and B are constant values that are collections of statistical quantities in Equation 6. Equation 8 shows that there is a log-linear relationship between reliability index β and the nominal factor of safety. By increasing the nominal factor of safety at time of design and keeping all other quantities the same, the margin of safety expressed as reliability index or probability of failure also increases. While this is expected, Equation 6 (or equivalently Equation 8) has the advantage of providing a quantitative link between deterministic factor of safety design practice and margins of safety expressed in a probabilistic framework.

RESULTS

Bias values for the load and resistance models in this investigation are summarized in Table 2. The data are "pooled data" collected by the authors and co-workers from multiple sources that can be traced through the references in the papers identified in the table. The data fall within the envelope of project conditions and material properties specified in the current North American codes for the construction of geosynthetic MSE walls. Similarly, the material properties were determined using accepted test methods. Uncertainty in the magnitude of nominal load and resistance values (as applicable) is quantified by COV of nominal values of 0, 0.1, 0.2, and 0.3 in the calculation of β to follow. The non-zero values can be associated with the notion of "level of understanding" explained earlier in the paper and adopted in Canadian foundation LRFD practice (Fenton et al. 2016; Bathurst et al. 2017). A value of zero can be understood to represent current U.S. practice where the concept of level of understanding is not used. Based on the project information available at the time of the SR-18 wall designs and the experience of the authors, the "level of understanding" for these walls would be judged "high." However, calculations are carried out for all levels of understanding to demonstrate the sensitivity of reliability index results to the range of nominal COV values from 0 to 0.3.

Table 3 summarizes the margins of safety for the tensile strength limit state in deterministic (factor of safety) and probabilistic terms (reliability index β) for each reinforcement layer in Walls C and D. The corresponding outcomes for the pullout strength limit state are reported in Table 4.

Table 3. Tensile strength limit state results for all reinforcement layers (COV_{Rn} = 0, ρ_n = 0).

a) Wall D

Layer	Depth, z (m)	$Q_n = T_{max}$ (kN/m)	$R_n = T_{al}$ (kN/m)	F_n	OFS	Reliability index, β			
						Level of understanding			
							High	Typical	Low
						COV_{Qn} = 0	COV_{Qn} = 0.1	COV_{Qn} = 0.2	COV_{Qn} = 0.3
10 (Top)	0.50	0.68	17.4	25.4	29.1	9.4	9.1	8.3	7.4
9	1.10	0.91	17.4	19.1	21.9	8.7	8.4	7.6	6.8
8	1.70	1.22	17.4	14.2	16.3	7.8	7.6	6.9	6.2
7	2.30	1.54	17.4	11.3	12.9	7.2	7.0	6.4	5.7
6	2.90	1.85	17.4	9.4	10.7	6.7	6.5	5.9	5.3
5	3.50	2.17	17.4	8.0	9.2	6.3	6.0	5.5	5.0
4	4.10	2.17	17.4	8.0	9.2	6.3	6.0	5.5	5.0
3	4.70	2.17	17.4	8.0	9.2	6.3	6.0	5.5	5.0
2	5.30	2.17	17.4	8.0	9.2	6.3	6.0	5.5	5.0
1	5.90	1.77	17.4	9.8	11.2	6.8	6.6	6.0	5.4

b) Wall C

Layer	Depth, z (m)	$Q_n = T_{max}$ (kN/m)	$R_n = T_{al}$ (kN/m)	F_n	OFS	Reliability index, β			
						Level of understanding			
							High	Typical	Low
						COV_{Qn} = 0	COV_{Qn} = 0.1	COV_{Qn} = 0.2	COV_{Qn} = 0.3
17 (Top)	0.7	1.14	17.4	15.2	15.0	8.0	7.8	7.1	6.3
16	1.3	1.21	17.4	14.3	14.2	7.9	7.6	6.9	6.2
15	1.9	1.54	17.4	11.3	11.1	7.2	7.0	6.4	5.7
14	2.5	1.87	17.4	9.3	9.2	6.7	6.4	5.9	5.3
13	3.1	2.20	17.4	7.9	7.8	6.2	6.0	5.5	4.9
12	3.7	3.19	19.8	6.2	7.0	5.6	5.4	4.9	4.4
11	4.3	3.61	19.8	5.5	6.2	5.2	5.0	4.6	4.1
10	4.9	4.02	19.8	4.9	5.6	4.9	4.8	4.4	3.9
9	5.5	5.48	32.5	5.9	6.7	5.4	5.3	4.8	4.3
8	6.1	5.99	32.5	5.4	6.1	5.2	5.0	4.6	4.1
7	6.7	6.50	32.5	5.0	5.6	5.0	4.8	4.4	4.0
6	7.3	6.52	32.5	5.0	5.6	5.0	4.8	4.4	3.9
5	7.9	6.52	32.5	5.0	5.6	5.0	4.8	4.4	3.9
4	8.5	6.52	32.5	5.0	5.6	5.0	4.8	4.4	3.9
3	9.1	6.52	32.5	5.0	5.6	5.0	4.8	4.4	3.9
2	9.7	6.52	32.5	5.0	5.6	5.0	4.8	4.4	3.9
1	10.3	5.32	32.5	6.1	6.9	5.5	5.3	4.9	4.4

Table 4. Pullout strength limit state results for all reinforcement layers ($COV_{Rn} = COV_{Qn}$, $\rho_n = -1$).

a) Wall D

Layer	Depth, z (m)	$Q_n = T_{max}$ (kN/m)	L_e (m)	$R_n = P_c$ (kN/m)	F_n	OFS	Reliability index, β			
							Level of understanding			
								High	Typical	Low
							$COV_{Qn} = 0$	$COV_{Qn} = 0.1$	$COV_{Qn} = 0.2$	$COV_{Qn} = 0.3$
10 (Top)	0.50	0.68	2.06	41.0	60.1	139.5	7.8	7.9	7.3	6.3
9	1.10	0.91	2.30	62.5	68.9	160.1	8.1	8.2	7.5	6.5
8	1.70	1.22	2.54	62.5	51.1	118.8	7.6	7.7	7.1	6.1
7	2.30	1.54	2.77	62.5	40.6	94.4	7.2	7.3	6.7	5.8
6	2.90	1.85	3.01	62.5	33.7	78.3	6.9	7.0	6.4	5.6
5	3.50	2.17	3.25	62.5	28.8	67.0	6.7	6.7	6.2	5.4
4	4.10	2.17	3.48	62.5	28.8	66.9	6.6	6.7	6.2	5.4
3	4.70	2.17	3.72	62.5	28.8	66.9	6.6	6.7	6.2	5.4
2	5.30	2.17	3.95	62.5	28.8	66.9	6.6	6.7	6.2	5.4
1	5.90	1.77	4.19	62.5	35.3	81.9	7.0	7.1	6.5	5.6

b) Wall C

Layer	Depth, z (m)	$Q_n = T_{max}$ (kN/m)	L_e (m)	$R_n = P_c$ (kN/m)	F_n	OFS	Reliability index, β			
							Level of understanding			
								High	Typical	Low
							$COV_{Qn} = 0$	$COV_{Qn} = 0.1$	$COV_{Qn} = 0.2$	$COV_{Qn} = 0.3$
17 (Top)	0.7	1.14	3.49	57.9	50.7	117.7	7.6	7.7	7.1	6.1
16	1.3	1.21	3.73	62.5	51.5	119.7	7.6	7.7	7.1	6.1
15	1.9	1.54	3.96	62.5	40.5	94.2	7.2	7.3	6.7	5.8
14	2.5	1.87	4.20	62.5	33.4	77.6	6.9	7.0	6.4	5.6
13	3.1	2.20	4.44	62.5	28.4	66.0	6.6	6.7	6.2	5.4
12	3.7	3.19	4.67	71.2	22.3	51.8	6.2	6.3	5.8	5.0
11	4.3	3.61	4.91	71.2	19.7	45.8	6.0	6.1	5.6	4.9
10	4.9	4.02	5.14	71.2	17.7	41.1	5.9	6.0	5.5	4.7
9	5.5	5.48	5.38	117.0	21.4	49.6	6.2	6.3	5.8	5.0
8	6.1	5.99	5.62	117.0	19.5	45.4	6.0	6.1	5.6	4.9
7	6.7	6.50	5.85	117.0	18.0	41.8	5.9	6.0	5.5	4.8
6	7.3	6.52	6.09	117.0	18.0	41.7	5.9	6.0	5.5	4.8
5	7.9	6.52	6.33	117.0	18.0	41.7	5.9	6.0	5.5	4.8
4	8.5	6.52	6.56	117.0	18.0	41.7	5.9	6.0	5.5	4.8
3	9.1	6.52	6.80	117.0	18.0	41.7	5.9	6.0	5.5	4.8
2	9.7	6.52	7.03	117.0	18.0	41.7	5.9	6.0	5.5	4.8
1	10.3	5.32	7.27	117.0	22.0	51.1	6.2	6.3	5.8	5.0

Reliability analyses for the tensile strength limit state were carried out with $COV_{Rn} = 0$ consistent with no uncertainty in the choice of nominal strength ($R_n = T_{al}$) of the reinforcement at the time of design. The uncertainty (or variability) in long-term tensile capacity of the reinforcement is quantified by the spread in bias values (i.e., $COV_{\lambda R}$) as noted earlier. The nominal tensile strength and reinforcement stiffness are related. Specifically, reinforcement stiffness ($J_{2\%}$) for the products used in this project has been demonstrated to increase linearly with T_{ult} (Allen and Bathurst 2019). However, because $COV_{Rn} = 0$, the magnitude of this nominal correlation (ρ_n) does not influence the magnitude of β in Equation 6. Examination of the load model (Equations 1a and 1b) and the pullout model (Equation 3) shows that there are common peak friction angle (ϕ) and vertical stress (σ_v) terms. As the friction angle increases, the tensile load T_{max} decreases and the pullout strength increases (negative correlation). As the vertical stress value increases, the magnitude of T_{max} and the pullout strength (P_c) increase (positive correlation). The most conservative outcome (i.e., lowest value of β) occurs when $\rho_n = -1$. This value has been used in the calculations for the pullout strength limit state. Regardless, all values of β can be seen to be well above magnitudes of practical concern as discussed next.

The factors of safety (F_n) and β values shown in Tables 4 and 5 are very large. These outcomes show that these limit states are satisfied by huge margins. For example, the factor of safety based on past practice for tensile strength and pullout strength internal stability limit states using the Simplified Method is equivalent to $F_n = \gamma_Q/\varphi = 1.35/0.90 = 1.5$ where γ_Q and φ are load and resistance factors respectively (AASHTO 2017). The excessive safety can also be appreciated when it is noted that the Stiffness Method was calibrated for LRFD using a target reliability index of β = 2.33 which corresponds to a probability of failure of $P_f = 1\%$ (e.g., Bathurst et al. 2019a). This value may appear to be very high. However, geosynthetic MSE walls are highly strength-redundant systems; hence, if one layer fails, there are other layers that can compensate (Allen et al. 2005). The same low reliability index value β = 2.33 is recommended for the ultimate compression capacity design of a single pile in a group of five piles or more (Zhang et al. 2001) based on the same assumption of multi-element strength redundancy.

The choice of reinforcement materials and the layer lengths at the time of the original design for these walls were controlled by other ultimate limit states: specifically, internal composite failure mechanisms, external sliding, and global stability associated with failure surfaces that pass behind, through, and below the reinforced soil zone. Furthermore, the range of HDPE geogrid products that were available in the product line selected for the project at time of design prior to wall construction in 2006 was limited to products with tensile strengths and stiffness that were greater than values required to satisfy the tensile strength limit state using the K-stiffness Method. The minimum total reinforcement length was also constrained by the prescriptive empirical criterion that $L \geq 0.7H$. This criterion results in excessive lengths of the anchorage length (L_e) in the passive zones, and these lengths increase with depth below the crest of the wall as shown in Figures 3 and 5.

Table 5 summarizes the margins of safety for the soil failure strength limit state in deterministic (factor of safety) and probabilistic terms (reliability index β) for each reinforcement layer in Walls C and D. In these calculations, ε_{max} was taken as 2% as recommended in AASHTO (2020) specifications for stiff-faced walls. This strain criterion results in conservative (lower) values of β compared to outcomes using $\varepsilon_{max} = 2.5\%$ for stiff-faced walls as recommended by the writers during the development of the (Simplified) Stiffness Method (Allen and Bathurst 2015). The reader is directed to WSDOT (2020) which contains useful guidance on the link between facing stiffness and reinforcement strain limits to maintain the integrity of the reinforced soil zone under working stress (operational) conditions. The values of $Q_n = T_{max}$ and $R_n = T_j$ are positive correlated. This is because as $J_{2\%}$ increases in Equation 4, the magnitude of T_J increases. Similarly, as $J_{2\%}$ increases, the reinforcement becomes stiffer (global stiffness factor, Φ_g, increases) and the tensile reinforcement load increases (Equation 1a and 1b). However, as was the case for the tensile strength limit state, because $COV_{Rn} = 0$, the magnitude of the nominal correlation (ρ_n) between load and resistance nominal values does not influence the magnitude of β in Equation 6; uncertainty in the magnitude of T_J is captured by the spread in bias of $J_{2\%}$ values ($COV_{\lambda R}$).

The factors of safety and reliability index presented in Table 5 are markedly lower for this limit state than the corresponding values for the tensile strength and pullout strength limit states. Allen and Bathurst (2018) recommended that the target reliability index for LRFD calibration for the soil failure limit state be taken as β = 1.0 ($P_f = 1/6$) which is consistent with serviceability limit states in structural engineering (Allen 2013; Azizinamini et al. 2014). They also recommended load and resistance factors of $\gamma_Q = 1.20$ and φ = 1.00, respectively. The ratio of these values gives an equivalent nominal factor of safety of $F_n = \gamma_Q/\varphi = 1.20/1.00 = 1.2$. Computed values of F_n and β in Table 5 approach the target minimum values noted above for some layers, but margins of safety are satisfied for all layers.

Table 5. Soil failure limit state results for all reinforcement layers (COV_{Rn} = 0, ρ_n = 1).

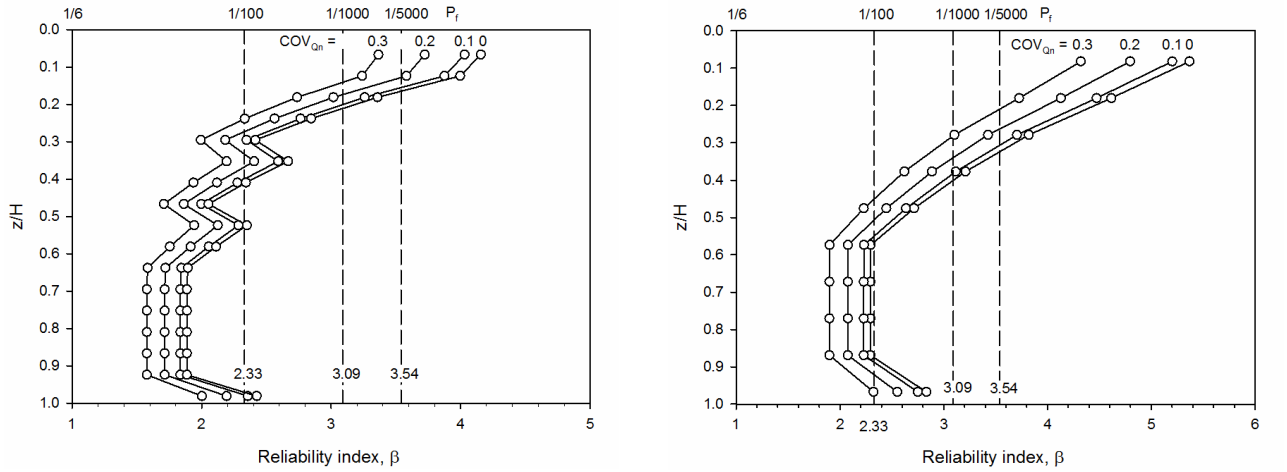
a) Wall D

Layer	Depth, z (m)	$Q_n = T_{max}$ (kN/m)	$R_n = T_J$ (kN/m) (ε_{max} = 2%)	F_n	OFS	Reliability index, β			
						Level of understanding			
							High	Typical	Low
						COV_{Qn} = 0	COV_{Qn} = 0.1	COV_{Qn} = 0.2	COV_{Qn} = 0.3
10 (Top)	0.50	0.68	4.6	6.8	7.1	5.4	5.2	4.8	4.3
9	1.10	0.91	4.6	5.1	5.4	4.6	4.5	4.1	3.7
8	1.70	1.22	4.6	3.8	4.0	3.8	3.7	3.4	3.1
7	2.30	1.54	4.6	3.0	3.2	3.2	3.1	2.9	2.6
6	2.90	1.85	4.6	2.5	2.6	2.7	2.6	2.4	2.2
5	3.50	2.17	4.6	2.1	2.3	2.3	2.2	2.1	1.9
4	4.10	2.17	4.6	2.1	2.2	2.3	2.2	2.1	1.9
3	4.70	2.17	4.6	2.1	2.2	2.3	2.2	2.1	1.9
2	5.30	2.17	4.6	2.1	2.2	2.3	2.2	2.1	1.9
1	5.90	1.77	4.6	2.6	2.8	2.8	2.8	2.6	2.3

b) Wall C

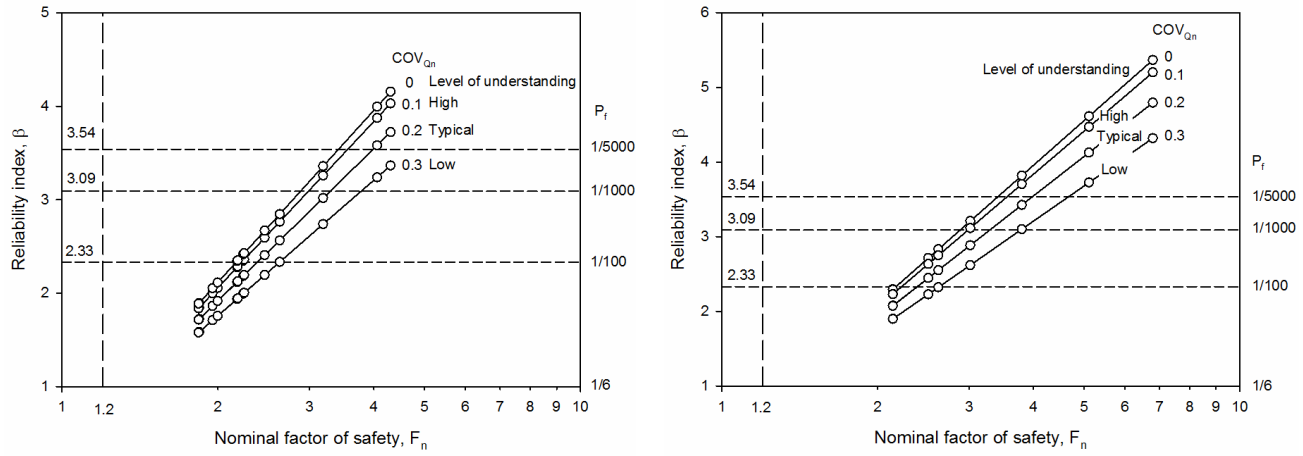
Layer	Depth, z (m)	$Q_n = T_{max}$ (kN/m)	$R_n = T_J$ (kN/m) (ε_{max} = 2%)	F_n	OFS	Reliability index, β			
						Level of understanding			
							High	Typical	Low
						COV_{Qn} = 0	COV_{Qn} = 0.1	COV_{Qn} = 0.2	COV_{Qn} = 0.3
17 (Top)	0.7	1.14	4.8	4.3	4.5	4.2	4.0	3.7	3.4
16	1.3	1.21	4.8	4.1	4.3	4.0	3.9	3.6	3.2
15	1.9	1.54	4.8	3.2	3.4	3.4	3.3	3.0	2.7
14	2.5	1.87	4.8	2.6	2.8	2.8	2.8	2.6	2.3
13	3.1	2.20	4.8	2.2	2.4	2.4	2.3	2.2	2.0
12	3.7	3.19	7.7	2.5	2.6	2.7	2.6	2.4	2.2
11	4.3	3.61	7.7	2.2	2.3	2.3	2.3	2.1	1.9
10	4.9	4.02	7.7	2.0	2.1	2.1	2.0	1.9	1.7
9	5.5	5.48	11.8	2.2	2.3	2.4	2.3	2.1	1.9
8	6.1	5.99	11.8	2.0	2.1	2.1	2.1	1.9	1.8
7	6.7	6.50	11.8	1.8	1.9	1.9	1.8	1.7	1.6
6	7.3	6.52	11.8	1.8	1.9	1.9	1.8	1.7	1.6
5	7.9	6.52	11.8	1.8	1.9	1.9	1.8	1.7	1.6
4	8.5	6.52	11.8	1.8	1.9	1.9	1.8	1.7	1.6
3	9.1	6.52	11.8	1.8	1.9	1.9	1.8	1.7	1.6
2	9.7	6.52	11.8	1.8	1.9	1.9	1.8	1.7	1.6
1	10.3	5.32	11.8	2.2	2.4	2.4	2.4	2.2	2.0

The distribution and magnitude of reliability index β are plotted with normalized depth of layer below the crest of the two walls in Figure 6. The most critical layers for this limit state are located in the lower half of the walls. The data show that as the magnitude of the uncertainty in the nominal load (COV_{Qn}) increases, the reliability index decreases (or probability that the limit state is not satisfied increases). The same data are plotted as reliability index versus nominal factor of safety in Figure 7. The plots present as linear lines using log-linear axes as expected using Equation 8. In all cases, the margin of safety exceeds the target nominal factor of safety of $F_n = 1.2$ and the probabilistic target of $\beta = 1$ (or $P_f = 1/6$). The data points in Figure 7b for each value of COV_{Qn} fall on the same line because the bias statistics for each reinforcement type are the same. The data at the lower end of the plots suggest that lower stiffness reinforcement products from the same product line could be safely used if such products were available. Finally, Figure 8 shows the operational factor of safety (OFS) plotted against the nominal factor of safety (F_n) using Equation 7. The plot shows that the operational factor of safety is (on average) about 5% greater than the nominal factor of safety for the soil failure limit state for all layers and both walls.



a) Wall C *b) Wall D*

Figure 6. Reliability index for soil failure limit state for reinforcement layers.



a) Wall C *b) Wall D*

Figure 7. Reliability index versus nominal factor of safety for soil failure limit state.

The main conclusions in this section for the two SR-18 walls using the as-built geogrid reinforcement, reinforcement arrangement, and backfill soil are a) the possibility of inadequate tensile strength or pullout strength is not a practical concern, b) soil failure is the most critical limit state, and c) while margins of safety for the soil failure limit state are closer to target minimum levels, they remain satisfactory.

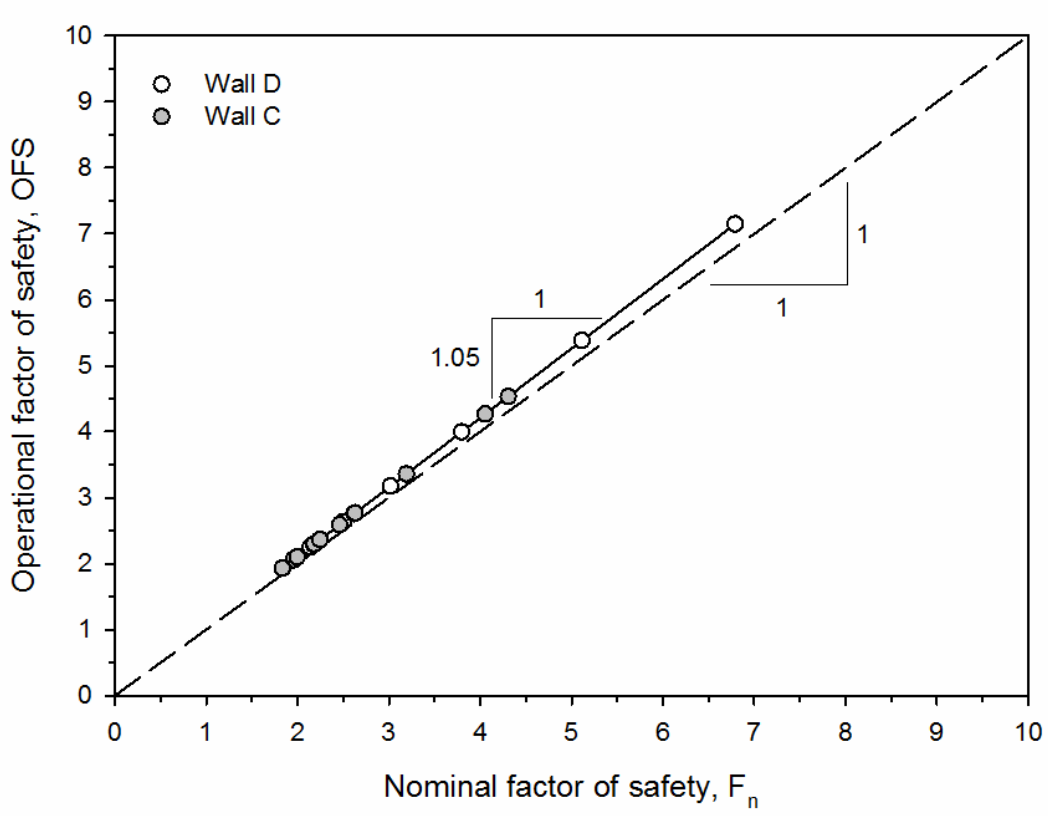


Figure 8. Operational factor of safety versus nominal factor of safety for soil failure limit state.

RELIABILITY ASSESSMENT USING A LOWER STRENGTH AND STIFFNESS GEOGRID

Recall that at the time of the original design of the SR-18 walls, the range of HDPE geogrid materials in the product line in the project specifications was limited. If lower strength and stiffness products had been available, then it would have been possible to reduce the as-built margins of safety for the tensile strength and pullout strength limit states reported thus far. This section imagines that this is the case for Wall D constructed with a weaker and more extensible HDPE geogrid product. The previous calculations revealed that the most critical limit state is the soil failure limit state. Hence, the hypothetical geogrid in this section was selected based on the soil failure limit state with β =1.0 and lowest level of understanding (i.e., COV_{Qn} = 0.3). The secant stiffness value at 2% strain and 1000 h to just meet this margin of safety is $J_{2\%}$ = 115 kN/m. For the HDPE geogrids in the product line used in the as-built walls, the corresponding ultimate strength is T_{ult} = 20.9 kN/m based on the ratio of $J_{2\%}/T_{ult}$ = 5.5 reported by Allen and Bathurst (2019). This strength is well below the ultimate strength available in the actual product line at the time of writing. In fact, there are no geosynthetic reinforcement products used in MSE walls today that have such low strengths based on product evaluation reports available through the AASHTO National Transportation Product Evaluation Program (NTPEP 2019a,b) in the U.S.A. Furthermore, such low strength products would likely be too fragile to survive installation during typical MSE wall construction.

Nevertheless, the calculations reported in the previous section were repeated with this hypothetical reinforcement product to compute margins of safety for the three limit states in the previous section and to show that, once again, it is the soil failure limit state that controls design. To carry out these calculations it was necessary to assume that the strength reduction RF = 3.6, as before, and that bias values reported in Table 2 are applicable. As noted above, the susceptibility of such a light geogrid product to installation damage would be greater and thus the reduction factor RF should be greater. However, keeping RF = 3.6 is judged reasonable for the purpose of this section. The pullout capacity would be expected to be lower as well but limited by the ultimate tensile strength of the reinforcement as before. Similarly, it could be argued that the reinforcement could be placed at greater spacing. However, current practice is to maintain a maximum spacing of twice the block (toe to heel) width regardless of reinforcement type so that the reinforced soil mass acts as a homogenous composite mass. By keeping these parameters the same as in the previous section, the influence of reinforcement strength and stiffness on margins of safety is isolated.

The results of all limit state calculations for Wall D are summarized in Table 6. Table 6c for the soil failure limit state confirms that the minimum target nominal factor of safety of F_n = 1.2 and reliability index β = 1.0 were not exceeded. Qualitative trends reported in the previous section are also preserved. The ratio of OFS/F_n remains 1.05, which is not unexpected because the mean bias values of $\mu_{\lambda R}$ and $\mu_{\lambda Q}$ for resistance and load terms, respectively, remain the same.

While the magnitude of nominal factor of safety and reliability index are notably lower in Table 6 compared to the corresponding values for the same limit states in the previous section, they remain large enough that failure to meet tensile strength and pullout strength limit states is not a practical concern using the imagined lower strength and stiffness geogrid.

Table 6. Wall D with $J_{2\%}$ = 115 kN/m and T_{ult} = 20.9 kN/m.

a) Tensile strength limit state (COV_{Rn} = 0, ρ_n = 0)

Layer	Depth, z (m)	$Q_n = T_{max}$ (kN/m)	$R_n = T_{al}$ (kN/m)	F_n	OFS	Reliability index, β			
						Level of understanding			
						High	Typical		Low
						COV_{Qn} = 0	COV_{Qn} = 0.1	COV_{Qn} = 0.2	COV_{Qn} = 0.3
10 (Top)	0.50	0.51	5.81	11.4	13.0	7.2	7.0	6.4	5.7
9	1.10	0.68	5.81	8.5	9.8	6.4	6.2	5.7	5.1
8	1.70	0.92	5.81	6.3	7.2	5.6	5.4	5.0	4.4
7	2.30	1.15	5.81	5.0	5.8	5.0	4.8	4.4	4.0
6	2.90	1.39	5.81	4.2	4.8	4.5	4.3	4.0	3.6
5	3.50	1.62	5.81	3.6	4.1	4.0	3.9	3.6	3.2
4	4.10	1.62	5.81	3.6	4.1	4.0	3.9	3.6	3.2
3	4.70	1.62	5.81	3.6	4.1	4.0	3.9	3.6	3.2
2	5.30	1.62	5.81	3.6	4.1	4.0	3.9	3.6	3.2
1	5.90	1.33	5.81	4.4	5.0	4.6	4.4	4.1	3.7

b) Pullout strength limit state ($COV_{Rn} = COV_{Qn}$, $\rho_n = -1$)

Layer	Depth, z (m)	$Q_n = T_{max}$ (kN/m)	L_e (m)	$R_n = P_c$ (kN/m)	F_n	OFS	Reliability index, β			
							Level of understanding			
							High	Typical		Low
							COV_{Qn} = 0	COV_{Qn} = 0.1	COV_{Qn} = 0.2	COV_{Qn} = 0.3
10 (Top)	0.50	0.51	2.06	20.9	41.0	95.2	7.2	7.3	6.7	5.8
9	1.10	0.68	2.30	20.9	30.7	71.4	6.8	6.9	6.3	5.5
8	1.70	0.92	2.54	20.9	22.7	52.8	6.3	6.4	5.9	5.1
7	2.30	1.15	2.77	20.9	18.2	42.2	5.9	6.0	5.5	4.8
6	2.90	1.39	3.01	20.9	15.0	34.9	5.6	5.7	5.2	4.5
5	3.50	1.62	3.25	20.9	12.9	30.0	5.4	5.4	5.0	4.3
4	4.10	1.62	3.48	20.9	12.9	30.0	5.4	5.4	5.0	4.3
3	4.70	1.62	3.72	20.9	12.9	30.0	5.4	5.4	5.0	4.3
2	5.30	1.62	3.95	20.9	12.9	30.0	5.4	5.4	5.0	4.3
1	5.90	1.33	4.19	20.9	15.7	36.5	5.7	5.8	5.3	4.6

Table 6 continued. Wall D with $J_{2\%}$ = 115 kN/m and T_{ult} = 20.9 kN/m.

c) Soil failure limit state (COV_{Rn} = 0, ρ_n = 1)

Layer	Depth, z (m)	$Q_n = T_{max}$ (kN/m)	$R_n = T_J$ (kN/m) (e_{max} = 2%)	F_n	OFS	Reliability index, β			
						Level of understanding			
							High	Typical	Low
						COV_{Qn} = 0	COV_{Qn} = 0.1	COV_{Qn} = 0.2	COV_{Qn} = 0.3
10 (Top)	0.50	0.51	2.3	4.5	4.7	4.3	4.1	3.8	3.5
9	1.10	0.68	2.3	3.4	3.6	3.5	3.4	3.2	2.9
8	1.70	0.92	2.3	2.5	2.6	2.7	2.6	2.4	2.2
7	2.30	1.15	2.3	2.0	2.1	2.1	2.1	1.9	1.8
6	2.90	1.39	2.3	1.7	1.7	1.6	1.6	1.5	1.4
5	3.50	1.62	2.3	1.4	1.5	1.2	1.2	1.1	1.0
4	4.10	1.62	2.3	1.4	1.5	1.2	1.2	1.1	1.0
3	4.70	1.62	2.3	1.4	1.5	1.2	1.2	1.1	1.0
2	5.30	1.62	2.3	1.4	1.5	1.2	1.2	1.1	1.0
1	5.90	1.33	2.3	1.7	1.8	1.7	1.7	1.6	1.5

CONCLUSIONS AND DISCUSSION

The implications of the reliability analyses outcomes in this study have major impact on the appreciation of the actual margins of safety for the three internal limit states for the two walls investigated using the (Simplified) Stiffness Method recommended in current AASHTO (2020) specifications. Most importantly, it is shown that the soil failure limit state is the most critical limit state, which is consistent with the findings reported by Allen and Bathurst (2019). This has also been shown to be true for polyester (PET) strap MSE walls based on a study of three as-built instrumented walls reported by Bathurst et al. (2020b). It is interesting to note that for these PET strap structures, the margins of safety for tensile and pullout limit states were lower and for some walls were in closer (but safe) proximity to recommended minimums. Hence, the excessive conservativeness in margins of safety for tensile and pullout limit states reported in this paper for the SR-18 walls may not be as great for other MSE wall types. Finally, it should be noted that another source of conservativeness for the internal stability design of the as-built walls is that a peak friction angle of 38° was assumed at the time of design, while post-construction testing of the granular fill revealed a value of 47°.

The general approach used in the current study to compute the reliability index for simple limit states using a probabilistic approach (e.g., Equation 6) is also applicable to MSE walls reinforced with inextensible steel grids and strips (Bozorgzadeh et al. 2020; Bathurst et al. 2019b, 2020a,b). However, the soil failure limit state does not apply to these structures because soil failure will not occur before the steel reinforcement has yielded.

As mentioned earlier, not all design limit states for the SR-18 MSE walls have been investigated in the current study; these include connection strength, composite failure mechanisms, global instability, and external sliding. Bias statistics for the connection strength limit state are not available at the time of this investigation in order to assess this limit state in a probabilistic framework. However, deterministic analyses for this limit state carried out by the writers have revealed that the soil limit state remains the most critical limit state. Finally, it should be noted that additional reinforcement loads can be expected due to earthquakes. Current practice in Washington state at the location of the SR-18 walls is to design for a peak ground acceleration of 0.5g (WSDOT 2020; AASHTO 2020).

ACKNOWLEDGMENTS

The work reported in this paper was part of a pooled fund research program supported by grants from the Natural Sciences and Engineering Research Council (NSERC) of Canada, the Ministry of Transportation of Ontario, the Department of

National Defence (Canada), and the following state departments of transportation in the U.S.A.: Alaska, Arizona, California, Colorado, Idaho, Minnesota, New York, North Dakota, Oregon, Utah, Washington, and Wyoming.

REFERENCES

Allen, T. M. 2013. "AASHTO geotechnical design specification development in the USA." *Modern Geotechnical Design Codes of Practice—Development, Calibration and Experiences, P. Arnold, G. Fenton, M. Hicks, T. Schweckendiek and B. Simpson, eds.*, IOS Press, Amsterdam, Netherlands, 243-260.

Allen, T. M. and Bathurst, R. J. 2002. "Observed long-term performance of geosynthetic walls and implications for design." *Geosynthetics International,* 9(5-6), 567-606.

Allen, T. M. and Bathurst, R. J. 2013. "Comparison of working stress and limit equilibrium behavior of reinforced soil walls." *Sound geotechnical research to practice, Honoring Robert D, Holtz II. A. W. Stuedlein and B. R. Christopher, eds.*, ASCE, Reston, VA, 500-514.

Allen, T. M. and Bathurst, R. J. 2014a. "Performance of a 11 m high block-faced geogrid wall designed using the K-stiffness Method." *Canadian Geotechnical Journal,* 51(1), 16-29.

Allen, T. M. and Bathurst, R. J. 2014b. "Design and performance of a 6.3 m high block-faced geogrid wall designed using the K-stiffness Method." *ASCE Journal of Geotechnical and Geoenvironmental Engineering,* 142(2), 04013016.

Allen, T. M. and Bathurst, R. J. 2015. "An improved simplified method for prediction of loads in reinforced soil walls." *ASCE Journal of Geotechnical and Geoenvironmental Engineering*, 141(11), 04015049.

Allen, T. M. and Bathurst, R. J. 2018. "Application of the Simplified Stiffness Method to design of reinforced soil walls." *ASCE Journal of Geotechnical and Geoenvironmental Engineering,* 144(5), 04018024.

Allen, T. M. and Bathurst, R. J. 2019. "Geosynthetic reinforcement stiffness characterization for MSE wall design." *Geosynthetics International,* 26(6), 592-610.

Allen, T. M., Bathurst, R. J., Walters, D. L., Holtz, R. D. and Lee, W. F. 2003. "A new working stress method for prediction of reinforcement loads in geosynthetic walls." *Canadian Geotechnical Journal*, 40(5), 976-994.

Allen, T. M., Nowak, A. S. and Bathurst, R. J. 2005. *Calibration to Determine Load and Resistance Factors for Geotechnical and Structural Design. Transportation Research Board Circular E-C079*, Washington, DC.

American Association of State Highway and Transportation Officials (AASHTO) 2020. *LRFD Bridge Design Specifications, 9th Ed.,* Washington, DC, USA.

American Association of State Highway and Transportation Officials (AASHTO) 2017. *LRFD Bridge Design Specifications, 8th Ed.,* Washington, DC, USA.

Azizinamini, A., Power, E. H., Myers, G. F. and Ozyildirim, H. C. 2014. *Bridges for service life beyond 100 years: Innovative systems, subsystems, and components*. SHRP 2 Report. Transportation Research Board, Washington, DC, USA.

Bathurst, R. J., Allen, T. M., Lin, P. and Bozorgzadeh, N. 2019a. "LRFD calibration of internal limit states for geogrid MSE walls." *ASCE Journal of Geotechnical and Geoenvironmental Engineering,* 145(11), 04019087.

Bathurst, R. J., Allen, T. M., Miyata, Y., Javankhoshdel, S. and Bozorgzadeh, N. 2019b. "Performance-based analysis and design for internal stability of MSE walls." *Georisk*, 13(3), 214-225.

Bathurst, R. J., Allen. T. M. and Walters, D. L. 2005. "Reinforcement loads in geosynthetic walls and the case for a new working stress design method." *Geotextiles and Geomembranes,* 23(4), 287-322.

Bathurst, R. J., Bozorgzadeh, N., Miyata, Y. and Allen, T. M. 2020a. "Reliability-based design and analysis for internal limit states of steel grid-reinforced mechanically stabilized earth walls." *Canadian Geotechnical Journal (in press),* (https://doi.org/10.1139/cgj-2019-0820).

Bathurst, R. J., Huang, B. and Allen, T. M. 2011. "Analysis of installation damage tests for LRFD calibration of reinforced soil structures." *Geotextiles and Geomembranes,* 29(3), 323-334.

Bathurst, R. J. and Javankhoshdel, S. 2017. "Influence of model type, bias and input parameter variability on reliability analysis for simple limit states in soil-structure interaction problems." *Georisk,* 11(1), 42-54.

Bathurst, R. J., Miyata, Y. and Allen, T. M. 2020b. "Deterministic and probabilistic assessment of margins of safety for internal stability of as-built PET strap reinforced soil walls." *Geotextiles and Geomembranes,* 48, 780-792.

Bathurst, R. J., Walters, D., Vlachopoulos, N., Burgess, P. and Allen, T. M. 2000. "Full scale testing of geosynthetic reinforced walls." *Proc. of Geo-Denver 2000*, ASCE Special Publication No. 103, Advances in Transportation and Geoenvironmental Systems using Geosynthetics, Denver, Colorado, 201-217.

Becker, D. E. 1996. "Eighteenth Canadian Geotechnical Colloquium: Limit states design for foundations. Part II: Development for the National Building Code of Canada." *Canadian Geotechnical Journal,* 33(6), 984-1007.

Bozorgzadeh, N., Bathurst, R. J., Allen, T. M. and Miyata, Y. 2020. "Reliability-based analysis of internal limit states for MSE walls using steel strip reinforcement." *ASCE Journal of Geotechnical and Geoenvironmental Engineering,* 146(1), 0401911.

Canadian Standards Association (CSA) 2019. *Canadian Highway Bridge Design Code. CAN/CSA-S6-19.*, Mississauga, Ontario, Canada.

Fenton, G. A., Naghibi, F., Dundas, D., Bathurst, R. J. and Griffiths, D. V. 2016. "Reliability-based geotechnical design in the 2014 Canadian Highway Bridge Design Code." *Canadian Geotechnical Journal,* 53(2), 236-251.

Huang, B. and Bathurst, R. J. 2009. "Evaluation of soil-geogrid pullout models using a statistical approach." *Geotechnical Testing Journal,* 32(6), 489-504.

Lin, P. and Bathurst, R. J. 2018. "Influence of cross-correlation between nominal load and resistance on reliability-based design for simple linear soil-structure limit states." *Canadian Geotechnical Journal,* 55(2), 279-295.

Miyata, Y., Bathurst, R. J. and Allen, T. M. 2018. "Evaluation of tensile load model accuracy for PET strap MSE walls." *Geosynthetics International,* 25(6), 656-671.

National Transportation Product Evaluation Program (NTPEP) 2019a.. "Use and Application of NTPEP Geosynthetic Reinforcement Test Results." American Association of State Highway and Transportation Officials (AASHTO), Washington, DC, USA. <https://www.ntpep.org/Documents/Technical_Committee/REGEO/REGEO_Geo-Reinforcement-Primer_Updated_5-09.pdf> (May 5, 2019).

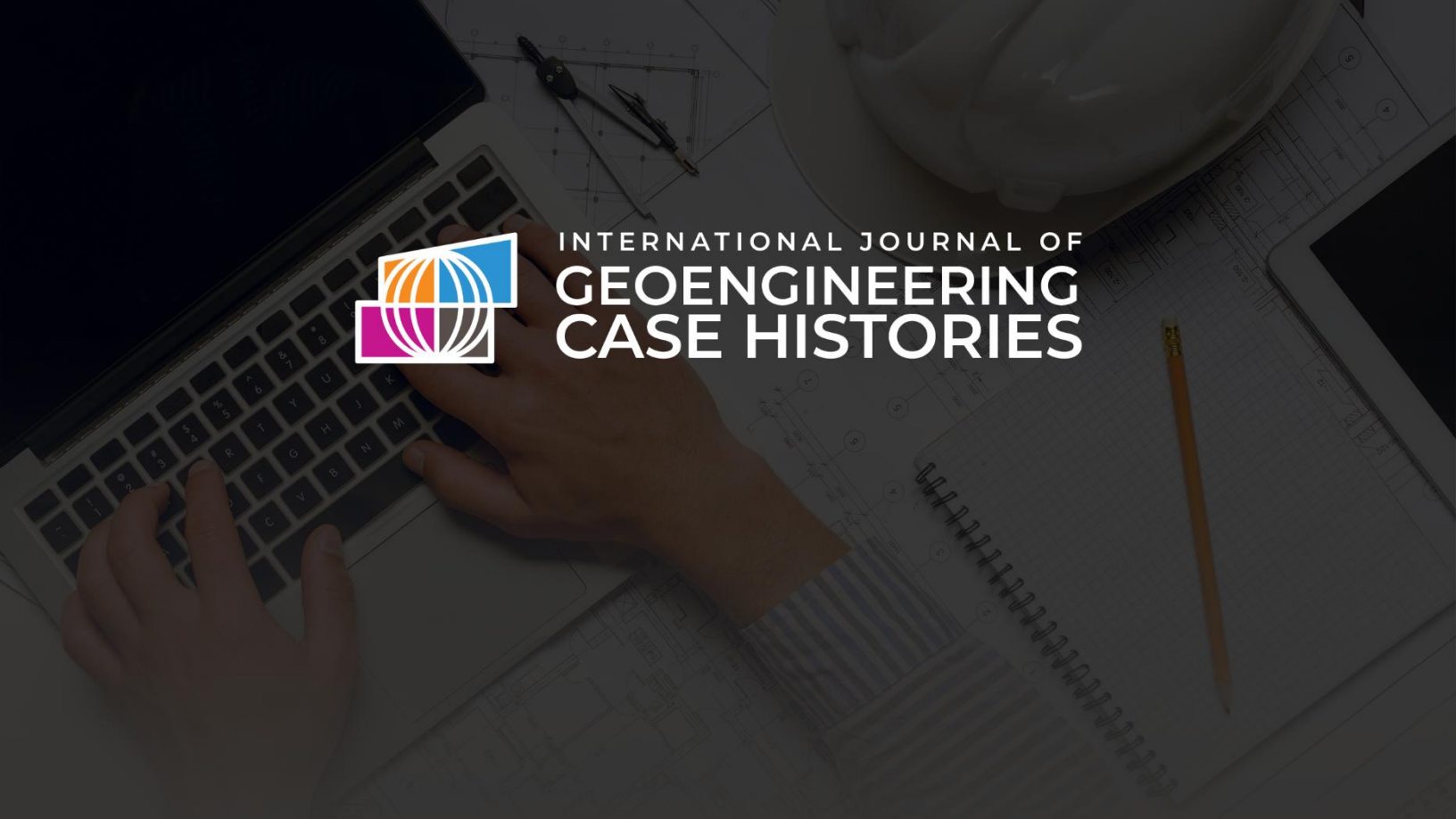
National Transportation Product Evaluation Program (NTPEP) 2019b. "DataMine – Geosynthetic Reinforcement (REGEO)." American Association of State Highway and Transportation Officials (AASHTO), Washington, DC, USA. <https://data.ntpep.org/REGEO/Products> (May 5, 2019).

Phoon K .K. and Tang, C. 2019. "Characterisation of geotechnical model uncertainty." *Georisk*, 13(2), 101-130.

Washington State Department of Transportation 2020. *Geotechnical Design Manual M46-03.09.*, Olympia, WA, USA.

Yu, Y., Bathurst, R. J. and Allen, T. M. 2016. "Numerical modelling of the SR-18 geogrid reinforced modular block retaining walls." *ASCE Journal of Geotechnical and Geoenvironmental Engineering,* 142(5), 04016003.

Zhang, L., Tang, W. H. and Ng, C. W. W. 2001. "Reliability of axially loaded driven pile groups." *ASCE Journal of Geotechnical and Environmental Engineering*, 127(12), 1051-1060.



INTERNATIONAL JOURNAL OF
GEOENGINEERING
CASE HISTORIES

The Journal's Open Access Mission is generously supported by the following Organizations:

dar
a Sidara company

Geosyntec consultants
engineers | scientists | innovators

CONETEC
MUD BAY DRILLING
LANKELMA
Geotech DRILLING

ENGEO
Expect Excellence

Access the content of the ĪSSMGE Īnternational Journal of Geoengineering Case Histories at:
www.geocasehistoriesjournal.org

Downloaded: Wednesday, November 11 2026, 12:23:08 UTC